Section 3:

BONE CHARACTERIZATION

Chapter 13

APPLICATION OF NON-LINEAR ELASTIC WAVE SPECTROSCOPY (NEWS) TO IN VITRO DAMAGE ASSESSMENT IN CORTICAL BONE

Marie Muller[1], Timothy J. Ulrich[2], Maryline Talmant[1], David Mitton[3], Pascal Laugier[1], and Paul A. Johnson[2]
[1]Université Pierre et Marie Curie-Paris 6, Laboratoire d'Imagerie Paramétrique, UMR CNRS7623, 15 rue de l'Ecole de médecine, F-75006, Paris, France
[2]Geophysics Group, Los Alamos National Laboratory, Los Alamos, NM 87544, USA
[3]Laboratoire de Biomécanique, CNRS, ENSAM, 151 Bd de l'Hôpital, 750013, Paris, France

ABSTRACT

This chapter reviews recent experimental findings applying non-linear dynamical techniques, termed non-linear elastic wave spectroscopy (NEWS), to infer progressive mechanical damage in human bone, in vitro. Standard measures of bone mechanical properties are compared where possible, including the quasi-statically derived stiffness and hysteresis. The goal is to explore whether or not the methods can ultimately be applied in vivo, for applications such as diagnosing and monitoring the progression of osteoporosis, as well as bone healing. It is shown that the NEWS methods are extremely sensitive to progressive damage, far more so than the other methods applied. The results are promising, and current discussion involves how to conduct similar experiments in vivo.

13.1 INTRODUCTION AND BACKGROUND

The non-invasive evaluation of bone biomechanical competence remains a challenge, despite the ever-growing number of physical and imaging tools available. Among existing techniques, vibration and wave propagation analysis have been found to be valuable diagnostic tools to assess bone quality. Assessment of mechanical properties of human bone in vivo by mechanical vibration analysis consists of determining the natural vibration frequencies, mode shapes and/or damping ratio. Two primary vibration techniques have been developed that excite vibrations in the bone to be measured over a frequency range of approximately 50 Hz to 1000 Hz [1]. In the first of these, termed the impulse frequency response (IFR) method, the excitation is provided by a hammer impact. In the second method, termed the bone resonance analysis (BRA) method, the measurement system consists of an electromechanical shaker which applies a sinusoidal driving force to the bone

via an impedance head. The resulting vibration is measured with an accelerometer. Using an appropriate model, the vibrational characteristics (e.g., resonance frequencies) can be related to properties of bone that may prove useful as an index of the strength. Jurist [2,3] was among the first investigators to present a theoretical basis and a measurement method for determining the resonance frequency of the ulna in vivo. Bending modes have been identified for long bones (e.g., ulna, tibia, femur) and the resonance frequencies have been related to bending or torsional stiffness using a simple beam model [2-8].

As a quantitative assessment technique, the vibrational response of long bones has been addressed by several researchers for the in vivo determination of bone mechanical characteristics. The potential of vibration analysis applied to bone has been investigated as a non-invasive method to assess the effect that osteoporosis may have on the mechanical properties as well. From in vivo vibration measurements of the tibia in a population of osteoporotic patients and age-matched controls, it was concluded that the bending rigidity (i.e., the product of the Young's modulus and the moment of inertia), calculated from the resonance frequencies in osteoporotic tibiae, was smaller in contrast to the control group [9, 10]. In other studies, the modal damping factor has been found to correlate with fracture energy measured with an impact test [11, 12].

The vibration response has also been used to monitor fracture healing. In particular, the sensitivity of resonance frequency and of different vibration modes to fracture healing has been extensively described [13-17]. Clinical studies reported in, for instance [15, 18], clearly indicate that resonance frequencies can be used clinically to assess the healing state of a fractured long bone. The resonance frequency was found to steadily increase during the process of callus consolidation in both in vitro and in vivo experiments [15, 16]. In 2006, Alizad et al [19] used the acoustic radiation force with an amplitude-modulated signal in order to induce low-frequency vibration in intact, fractured, and bonded excised rat femurs. This study demonstrated that the presence of damage in the samples was responsible for a modification of the vibrational characteristics of the samples, resulting in a decrease of the resonance frequency. A numerical study reported shifting of the vibration spectrum due to fracture, as well as a stronger coupling between lateral and axial vibration spectra [20]. Bending stiffness of long bones was found to be more sensitive to healing than torsional stiffness or resonance frequency [21]. The above studies concur in suggesting that bone macro-damage (fracture) may potentially be assessed by measuring bone vibrational properties.

Another application of bone vibration analysis is the detection of peri-implant conditions. Hip prosthesis loosening can be determined in vivo by the analysis of the vibration of the implant. The excitation vibration is applied to the femoral condyle and the response measured at the great trochanter. The method characterizes changes with implant fixation stability of the complete spectral response of the prosthesis [22, 23]. Rosenstein et al [22] were the first to suggest that loosening may be detectable from the non-linear response of the implant: The vibration of a loose implant exhibits the presence of harmonics of the input frequency when the vibration response of a secure prosthesis matches that of the input vibration. Another resonance technique, which is also used for dental implants, consists in measuring the resonance frequency [24, 25] for the evaluation of the implant stability.

At higher frequencies (approximately 100 kHz to 2 MHz), linear characteristics of ultrasonic wave transmission through bone, such as frequency-dependent attenuation and speed of sound, are widely used to assess skeletal status and predict osteoporotic fracture risk. The use of ultrasonic wave transmission can be classified into two categories according to the experimental setup: namely, transverse transmission with the ultrasonic emitter and receiver placed on opposite sides of a skeletal site to be measured; and axial transmission with the emitter/receiver set placed parallel to the bone longitudinal axis on one side of a long bone [26]. The clinical potential of ultrasound for the investigation of pathological conditions that affect bone strength was recognized as early as in the late 1950s by Siegel

et al [27], who reported the first use of axial transmission for monitoring fracture healing at the tibia. Modern bone quantitative ultrasound was described in 1984 by Langton et al [28], who measured the slope of the frequency-dependent attenuation at the calcaneus to discriminate osteoporotic from non-osteoporotic women. Since then, many advances have been achieved and a variety of different sophisticated technologies capable of measuring different skeletal sites such as the heel, fingers, wrist or tibia have been introduced and evaluated [26]. Heel quantitative ultrasound (QUS) parameters are highly correlated with bone mineral density in most cases and predict future fracture risk almost as well as for central dual energy X-ray absorptiometry of the spine or hip [29]. Whereas vibration analysis yields information on whole-bone characteristics (e.g., bending rigidity), ultrasound analysis indicates local changes in bone properties (bone mineral density, microstructure, stiffness) of the segment of bone that is traversed by ultrasound [30-32].

Vibration and ultrasonic analysis of bone have thus been shown to be sensitive to bone conditions that affect bone strength such as osteoporosis or fracture (i.e., macro-damage); however, to the knowledge of the authors, no data is available regarding direct detection of micro-damage using vibrational techniques, likely due to the fact that the elastic parameters assessed in the studies mentioned above fail to be sensitive to discontinuities at the meso or micro scale (e.g., [33]).

Daily physiological loads resulting from walking, lifting, and weight bearing result in bone in local strains in a range of 0.05% to 0.3%, that are responsible for the generation of bone micro-cracking. Following Wolff's law, stating that bone structure is permanently adapting to the applied stresses [34], fatigue damage initiates a bone remodeling process designed to heal micro-damage. In healthy bone, remodeling contributes to bone stiffness and toughness, allowing bone to absorb energy without failing. Fracture risk is increased when an imbalance takes place between micro-damage factors (brittleness, porosity, softness), and bone remodeling [35]. Such imbalances can occur with bone age or with the development of osteoporosis. As a consequence, aged or osteoporotic bone exhibits more micro-damage than young and healthy bone [36]. Micro-crack accumulation has been observed in subjects older than 40 years, and micro-crack density and length show an approximate exponential increase with increasing age [34, 37-39]. Of note is that at the hip, micro-crack density is twice as large for 78-year-old women than for 46-year-old women [40] underscoring the effect of bone age on fragility.

Two hypotheses may explain observed crack accumulation as a function of age. In the first, it may be due to bone age and local hypermineralization of the bone matrix. Although osteoporotic bone is highly porous and globally less dense than normal bone, its mineral content can be locally high, due to bone age. Indeed, in some regions with a low remodeling rate, osteocytes go through their lifetime (around 25 years) without being subject to remodeling [36], and accumulate in the form of necrosed cells in the lacunae, preventing further remodeling. This leads to local hypermineralization and therefore a locally increased brittleness. Thus, aged and osteoporotic bone is locally highly brittle, in addition to being subjected to locally high stresses, because of its increased porosity. Damage can then accumulate in the form of micro-cracks that can lead to the formation of large-scale fractures [38]. Local bone age has been found to be much more important in a population of fractured subjects than in a control (non-fractured) population [36]. In the second hypothesis, damage accumulation may be due to an abnormally high remodeling rate, responsible for a considerably increased porosity, and therefore, for a higher stress concentration [40]. Micro-damage accumulation is thus potentially the result of an ensemble of complex phenomenon.

Bone micro-damage accumulation has important consequences on bone mechanical properties. It has been shown that micro-damage accumulation coincides with a decrease of bone toughness and stiffness [41-43]. Thus, micro-damage accumulation and bone fragility are strongly correlated. The accumulation of bone micro-damage has been proposed as one factor that contributes to increased skeletal fragility with age and that may increase the

risk for fracture in older women. Therefore, bone micro-damage characterization in vivo could indeed provide relevant information in terms of bone quality and thus fracture risk and skeletal fragility assessment.

Micro-damage can typically be quantitatively assessed invasively using histomorphometry [44-46]. In addition, newly developed high-resolution imaging techniques such as synchrotron radiation micro-computed tomography (SR-μCT) have been shown to be useful to assess micro-damage [47]. These methods provide very high resolution (up to a few microns using SR-μCT and less than a micron for histomorphometry) and are able to monitor damage accumulation during fatigue, either by placing a fatigue testing device in the synchrotron beam, or by using different fluorochromes for different fatigue states. Clearly, however, these techniques cannot be used in vivo. For instance, the resolution needed for micro-damage imaging requires lethal radiation levels, up to 28 keV in cortical bone. In addition, both techniques provide only local information, not necessarily indicative of the global or volumetric damage state.

Elastic non-linear parameters derived from dynamic wave studies show great sensitivity to damage in a variety of materials [48-52]. Indeed, damaged materials have proved to exhibit characteristic non-linear behaviors that can be used to infer material mechanical integrity. The physical basis of the behavior is related to damage features at scales apparently ranging from 10^{-9} to at least 10^{-1} m (e.g., [53]). Damage, in the form of distributed or localized cracks for instance, results in predictable characteristics of the vibration spectrum. For example, under resonance conditions, the resonance frequency (proportional to the modulus and wave speed) has been shown to shift downward with increasing vibration amplitude, due to the presence of the mechanical damage [48]. The authors note that, in 2002, Lee et al [54] used resonance ultrasound spectroscopy (RUS) to characterize bone linear elastic moduli. However, in this study, only linear parameters were assessed and bone micro-damage was not quantified. Another important manifestation of non-linear dynamic behavior is the fact that in the presence of two pure frequency waves, wave multiplication takes place leading to the presence of sum and difference frequencies (sidebands) as well as harmonics of each wave [49, 50]. The general group of methods, all relying on monitoring spectral components for extracting the elastic non-linear behavior, is termed non-linear elastic wave spectroscopy [49-51].

In the following, feasibility studies conducted by our groups are reviewed, demonstrating the sensitivity of non-linear dynamical parameters to progressively accumulated micro-damage in vitro. In the first part is described the origin of elastic non-linearity followed by a broadly applied theory that describes the elasticity of damaged solids. Following this, experimental protocols and results for the methods presented are shown. The first method, a resonance technique known as non-linear resonant ultrasound spectroscopy (NRUS) [48, 51], is based on the measurement of a resonance frequency shift with increasing vibration amplitude, and is applied to characterizing progressive damage in a population of human femurs. This is followed by progressive damage observations obtained from a modulation method, known as non-linear wave modulation spectroscopy (NWMS) [48, 50], in a single human femur. Following this a discussion and conclusions are presented. The results shown are derived primarily from previous studies by the authors groups [55, 56].

13.2 INTRODUCTION TO ELASTIC NON-LINEARITY

As noted, NEWS methods have their basis in monitoring the material elastic modulus in response to dynamic wave excitation, usually by measurement of wave distortion characteristics and their associated spectral components. In undamaged solids, most materials have small elastic non-linear response due to intrinsic anharmonicity of, for instance, the crystalline lattice-atomic level vibration. This contribution to elastic non-linearity is difficult to

measure, and its net effect is to *increase* the material modulus under dynamic oscillatory wave forcing. In a mechanically damaged material there is an additional contribution to the material elastic non-linearity due entirely to the damage itself. It has a different physical origin. The contribution is much larger than that of the anharmonicity, by at least one to two orders of magnitude. Cracks and other soft features in the material cause the material modulus to *decrease* under dynamic forcing: As wave amplitude increases progressively, the material modulus decreases accordingly (i.e., the material softens), depending on the strength or magnitude of the material non-linear parameter(s). The non-linear parameter(s) has/have been empirically related to mechanical damage intensity in a number of studies (e.g., [57-59]). There is no direct analytical relationship between damage intensity and the non-linear parameter(s), however, because the basic physics of dynamic wave/crack interaction is not well understood (e.g., [60]). In fact, there is no direct correlation with mechanical damage in most non-destructive testing methods. Normally, a damage/undamaged result is all that is required, or empirical relations are developed so that correlation between what is measured and damage intensity can be inferred. For the moment, phenomenological models are relied on to describe the elastic behaviors, including the damage characteristics, of these materials. Thus, the non-linear parameters defined in such models are indicative of damage intensity but not a direct measure of them.

13.3 THEORY

Following the phenomenological description of stress-strain developed by Guyer and McCall [61-64], the one-dimensional constitutive relation between the stress σ and the strain ε can be expressed in a first approximation as,

$$\sigma = \int C(\varepsilon, \dot{\varepsilon})\, \mathrm{d}\varepsilon \tag{13 – 1}$$

where C is the modulus and $\dot{\varepsilon} = \mathrm{d}\varepsilon/\mathrm{d}t$ is the strain rate. The modulus is strain-amplitude and strain-rate-dependent, and is defined as,

$$C(\varepsilon, \dot{\varepsilon}) = C_0(1 + \beta\varepsilon + \delta\varepsilon^2 - \alpha(\Delta\varepsilon + \varepsilon\,\mathrm{sign}(\dot{\varepsilon})) + \cdots) \tag{13 – 2}$$

where C_0 is the linear modulus, ε is the *instantaneous* strain amplitude in an oscillating wave, $\Delta\varepsilon$ is *maximum* (one half-peak) strain amplitude over the previous period ($\Delta\varepsilon = (\varepsilon_{\max} - \varepsilon_{\min})/2$ for continuous sine wave excitation), and the function $\mathrm{sign}(\dot{\varepsilon}) = 1$ for $\dot{\varepsilon} > 0$ and $\mathrm{sign}(\dot{\varepsilon}) = -1$ for $\dot{\varepsilon} < 0$. The $\mathrm{sign}(\dot{\varepsilon})$ function accounts for hysteresis in the stress-strain response of a propagating or standing wave. The parameter α is a measure of the hysteresis in stress-strain over a half wave cycle. The wave literally follows a small hysteresis loop in stress-strain as a function of time. The parameters β and δ are the classical non-linear coefficients in the Taylor expansion of stress versus instantaneous strain [65]. They indicate that the modulus is strain amplitude dependent (over the wave cycle). In a classical medium like water or many single crystals, only β and δ appear and they are very small in magnitude, meaning there is very little change in the modulus with dynamic strain amplitude.

In a cracked or otherwise damaged material, β and δ are normally at least 1 to 2 orders of magnitude larger than classical media, and are negative in value (in contrast to classical media). This means that the material modulus (and thus wave speed) *decreases* as wave strain amplitude increases, in contrast to classical media, where modulus and wave speed generally increase with strain amplitude. In addition, the presence of hysteresis gives distinctive attributes to the waveform and associated wave spectrum, and to the strain amplitude dependencies of harmonics versus the fundamental drive amplitude, as well as the resonance frequency. Since a wave is normally characterized in terms of its half-peak strain

amplitude $\Delta\varepsilon$ (or RMS strain), in a classical non-linear medium, a strain wave of frequency f_1 and amplitude $\Delta\varepsilon$ can transform into a strain wave containing frequency components $2f_1$, $3f_1$, etc., with strain amplitudes proportional to $(\Delta\varepsilon)^2$, $(\Delta\varepsilon)^3$, etc. In the case of a purely hysteretic material, the second harmonic cannot be generated ($\beta = 0$), and the third harmonic is predicted and observed to be quadratic with the strain amplitude of the fundamental, ($\Delta\varepsilon_{3f_1} \propto \alpha\Delta\varepsilon_{f_1}^2$). This implies that hysteresis acts as a second-order non-linearity. In medium where two sine waves $\Delta\varepsilon_1 \cos(2\pi f_1 t)$ and $\Delta\varepsilon_2 \cos(2\pi f_2 t)$ (ignoring the phase $kx=\phi$) are present, the waves multiply leading to new waves that have frequencies $f_1 \pm f_2$ with strain amplitudes proportional to $\beta\Delta\varepsilon_1\Delta\varepsilon_2$. When dynamic hysteresis dominates, due to the presence of mechanical damage in particular, the second-order sidebands ($f_1 \pm 2f_2$) will display strain amplitudes proportional to $\alpha\Delta\varepsilon_1\Delta\varepsilon_2$.

When a pure continuous wave (cw) frequency is applied to a sample simultaneously with an impulsive force that excites a number of the normal modes, the modes multiply with the cw frequency due to the β and α terms in Eqs. (13-1) and (13-2). Many sum and differences are created in this manner, and it tends to be a very robust approach to extracting the non-linear response of a material. The work presented that follows takes advantage of this approach, known as non-linear wave modulation spectroscopy.

In resonance, it can be shown that the resonance frequency f is proportional to the peak strain amplitude $\Delta\varepsilon$ via the non-linear parameter α,

$$\frac{\Delta f}{f_0} = \frac{f - f_0}{f_0} \approx \alpha\Delta\varepsilon \qquad (13-3)$$

where f_0 is the linear (low-amplitude) resonance frequency. This equation is the basis for non-linear resonant ultrasound spectroscopy, where the frequency of the resonance peak is followed with increasing strain amplitude in order to extract α. Note that the fundamental resonance frequency is related to the wave speed and modulus. For instance, in Young's mode resonance, the wave speed c is related to f_0 and sample length L,

$$c = f\lambda = 2f_0L = \sqrt{\frac{C}{\rho_0}} \qquad (13-4)$$

where ρ_0 is density in the unperturbed state. Thus, as frequency downshifts, the material modulus and wave speed decrease.

13.4 EXPERIMENTS

The overall approach outlined below was to progressively damage bone samples and measure their elastic non-linear response by applying NRUS or using NWMS, as a function of induced damage. In the following the samples and experiment are described.

13.4.1 Samples

The mid-distal part of 18 fresh human femurs obtained from cadavers (5 female and 13 male donors, mean = 81 years, SD = 13 years, range = 47 to 100 years; see Table 13-1) were assessed in the study. Samples were cut to leave 6-cm segments of the diaphysis (see Fig. 13-1 for cross-sectional view). Soft tissue was removed and the specimens were kept frozen at –20°C before measurement sessions. Specimens were then measured at room temperature, and were kept hydrated during the duration of the experiment. The ethical approval for the collection of samples was granted by the Human Ethics Committee of the

TABLE 13-1. Age and gender data for the samples used in the NRUS study. A single sample (70-year-old female) was available for the NWMS measurements

Sample # (j)	Age (yr)	Gender (M/F)	Sample # (j)	Age (yr)	Gender (M/F)
1	64	M	10	74	M
2	70	M	11	96	F
3	47	M	12	89	F
4	74	M	13	47	M
5	80	M	14	70	M
6	89	F	15	69	M
7	83	M	16	83	M
8	96	F	17	100	F
9	80	M	18	88	M

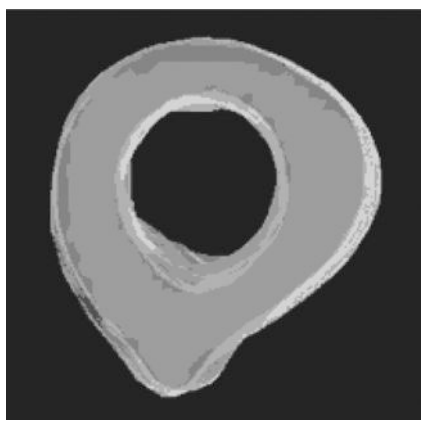

Figure 13-1. Cross section of the sample, a 6-cm tall (out of the plane of the figure) section of cortical bone taken from a human diaphysis (femur). The average outer diameter of the cross-section is approximately 2.5 cm. Similarly shaped and sized samples were used for all NRUS and NWMS experiments presented herein

Institute of Anatomy at the University René Descartes (Paris, France). The tissue donors or their legal guardians provided informed written consent to provide their tissues for investigation, in accord with legal clauses stated in the French Code of Public Health (Code de la Santé Publique Français).

13.4.2. Experimental Protocol

Fatigue damage was progressively induced in the specimens applying compressive mechanical testing (INSTRON 8500, Massachusetts, USA). For the samples subjected to the NRUS experiment, fatigue cycling was performed at 4 Hz (see Table 13-2). The cyclic load was determined for each sample, in order to induce a constant quasi-static strain amplitude: 0.5% for the samples from female donors older than 81 years (this is the median age for hip fracture for women, and thus a lower strain was determined to be appropriate in order to avoid early failure). For the other donors a 0.6% strain was applied. For the progressive damage study using NWMS, the fatigue cycling was done at a strain amplitude of 0.5% at 4 Hz.

TABLE 13.2. Damage step parameters for the progressive damage studies

Study	# Damage Steps (N)	# Cycles per Damage Step	Strain ($\Delta\varepsilon$)	Strain Rate (Hz)
NRUS	10	15,000	0.6%, (0.5%)[1]	4
NWMS	5	30,000	0.5%	4

[1]The quasi-static strain $(\varepsilon)^s$ was reduced to 0.5% for female samples age 81 yr and older.

To facilitate the discussion of the details of the experiments and results a notation is defined as follows:

- M = number of samples ($M_{\text{NRUS}} = 18$, $M_{\text{NWMS}} = 1$).
- N = number of damage steps ($N_{\text{NRUS}} = 10$, $N_{\text{NWMS}} = 5$).
- $i = 0,\ldots, N$, damage step designation ($i = 0$ indicates initial undamaged state).
- $j = 1,\ldots, M$, sample designation index.
- $F_{i,j}$ = applied loads during damage step i in sample j.
- $X_{i,j}$ = induced displacements for ith damage step and jth sample.
- $H_{i,j}$ = hysteresis measurements (i.e., area of hysteresis loops).
- $R_{i,j}$ = NRUS measurements.
- $K_{i,j}$ = stiffness measurement (from quasi-static $F_{i,j}$ and $X_{i,j}$ data).
- W_i = NWMS measurement at ith damage step (j is ignored as $j = 1$ for all NWMS experiments).
- $\alpha_{i,j}$, α_i, β_I, and Γ_i are non-linear parameters calculated from the data $R_{i,j}$ or W_i.

The procedure for the NRUS and NWMS studies began with the initial dynamic measurement ($R_{0,j}$ or W_0) for all samples to determine the initial non-linearity of the material. The samples were then taken through a damage step, consisting of cyclic loading as described above (also shown in Tab. 2), during which the quasi-static measurements of $F_{i,j}$ and $X_{i,j}$ were made and the stiffness $K_{i,j}$ determined. The quasi-static hysteresis $H_{i,j}$ was also measured, if observed. After each damage step a non-linear elasticity experiment was conducted ($R_{i,j}$ or W_i).

13.4.3 Non-Linear Resonant Ultrasound Spectroscopy

To perform the resonance measurements a piezo-ceramic source (with an 8-cm-thick steel backload bonded with epoxy) was attached to the samples using phenol salicilate. Frequency sweeps with progressively increasing amplitude were performed using an apparatus from Dynamic Resonance Systems, Inc. (Powell, WY, USA). The resulting displacements at the surface of the sample were measured using a laser interferometer (BMI, SH120, France). The NRUS experimental configuration is shown in Fig. 13-2.

In the NRUS measurements, the $R_{i,j}$ data consists of a suite of resonance curves, e.g., a single resonance peak excited with increasing drive amplitudes. Figure 13-3 displays two suites of resonance curves at two different damage states $i = 0$ and $i = 8$. From the resonance peak data $R_{i,j}$ the non-linear parameter $\alpha_{i,j}$ can be calculated by using Eq. (13-3). Preliminary feasibility studies of the NRUS technique for bone damage assessment were demonstrated in bovine bone in a previous study [66].

13.4.4 Non-Linear Wave Modulation Spectroscopy

This technique has been applied broadly in industrial materials and geomaterials (e.g., [50, 51]). In this feasibility study, only one sample was available for testing. For the NWMS experiments in human cortical bone, the sample was bonded to the piezoelectric source in

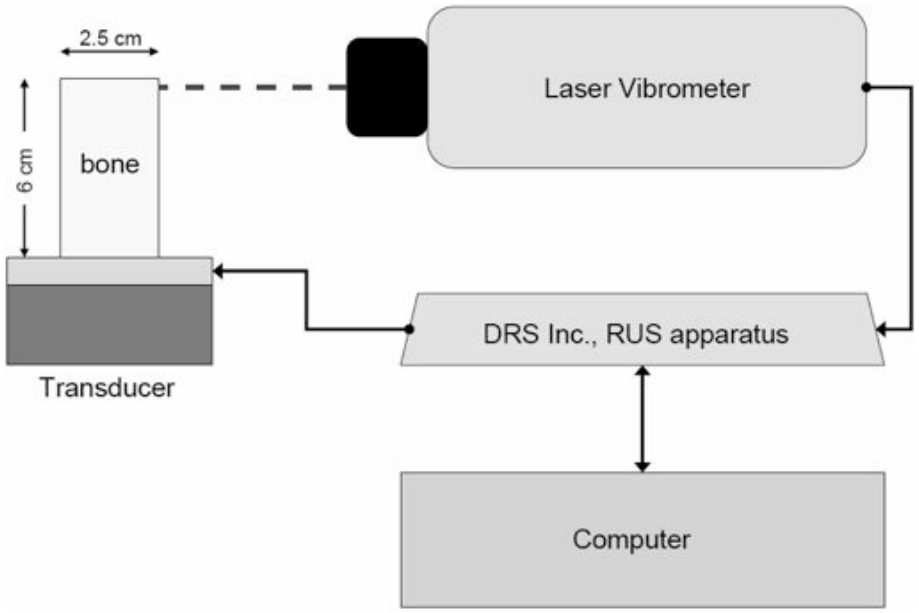

Figure 13-2. Non-linear resonant ultrasound spectroscopy experimental setup

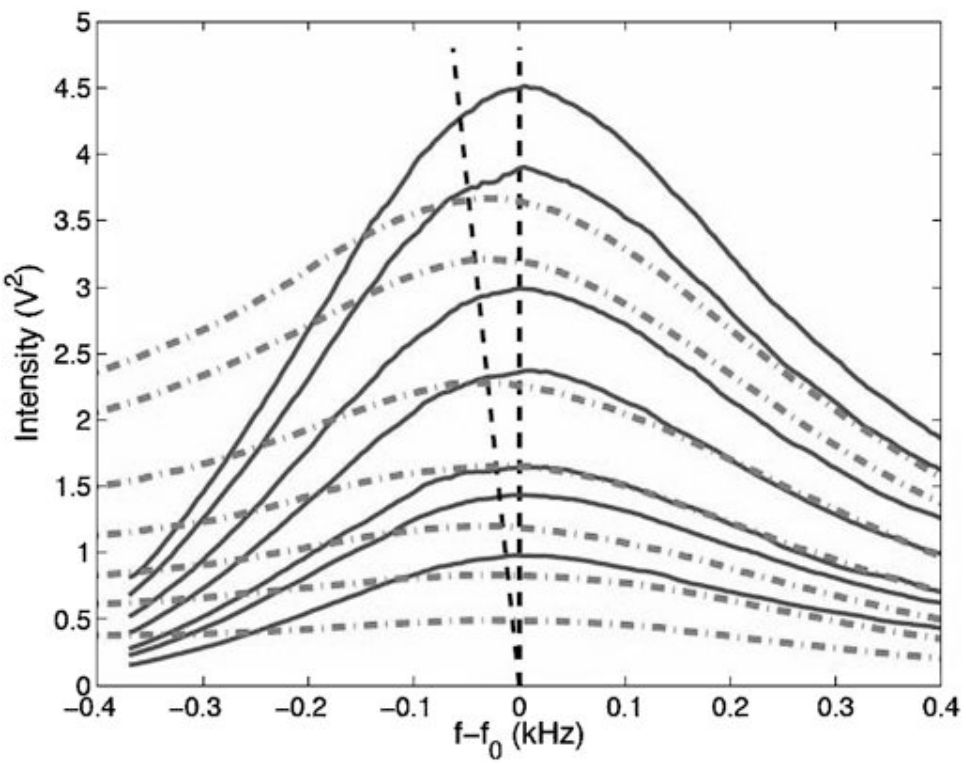

Figure 13-3. Resonance curves for a single sample at damage steps 0 (solid) and 8 (dot-dash). The shift of the resonance frequency is measurably more pronounced in the higher states of damage

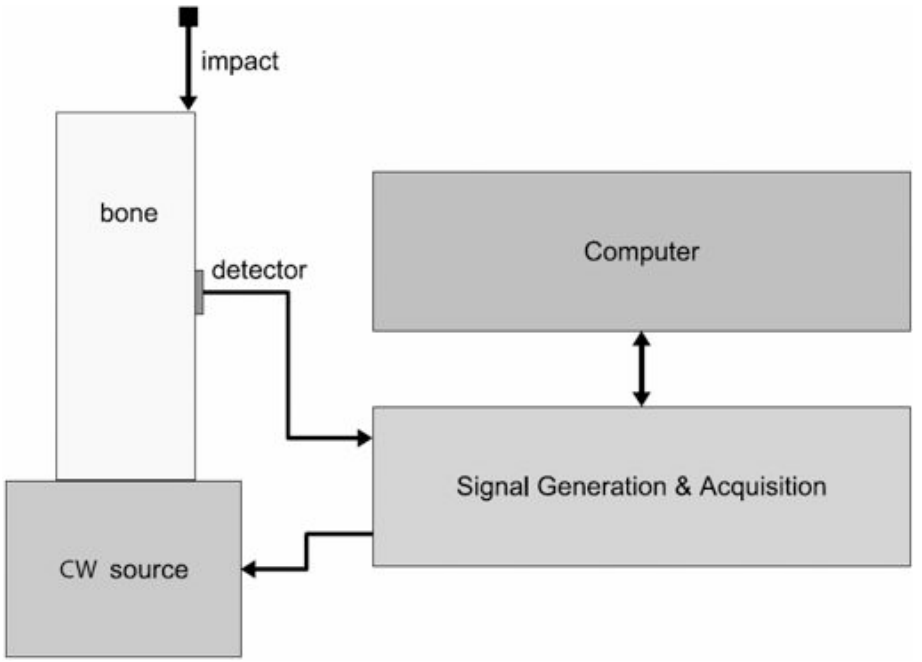

Figure 13-4. Non-linear wave modulation spectroscopy experimental setup. Signal generation and acquisition system consists of a 12-bit D/A converter (max. conversion rate, 150 MS/sec; max. output level, 50 V_{pp}) and a 14-bit A/D acquisition card

the same manner as was done for the NRUS measurements. The piezoelectric source was driven at a continuous amplitude pure tone of 223 kHz to optimize the efficiency of the source and receiver bandwidth. The low-frequency vibrational modes of a bone sample were simultaneously excited by a mechanical impulse (induced by a light tap with a pen). The receiver was bonded midway between the ends of the sample as shown in Fig. 13-4. To obtain various excitation amplitudes, the intensity of the impulse and pure tone were systematically varied (30 excitation combinations at each damage level); however, lack of calibration prevents the actual strain amplitudes from being known. Without calibration, it was necessary to look only at relative changes of the non-linear parameters from their initial values in the undamaged state.

A dynamic non-linear parameter Γ_i, a function of α_i and β_i, was defined and obtained by integrating the frequency spectrum containing the first-order ($f_1 \pm f_2$) and second-order ($f_1 \pm 2f_2$) sidebands in order to include the effects of multiple sidebands simultaneously. The frequency range used for this study was 215 kHz to 231 kHz. In addition, the values of the non-linear parameters β_i and α_i were calculated from the ratio of the first- and second-order sideband amplitudes, respectively, to the product of the source amplitudes (i.e., A_1A_2).

13.5 RESULTS

13.5.1 NRUS Observations

Figure 13-5 shows load versus displacement curves for a test sample taken to failure under larger loading conditions, illustrating the well-known quasi-static non-linear and hysteretic

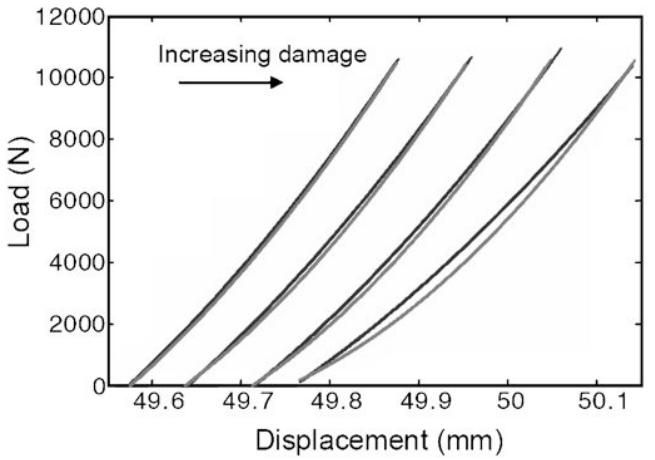

Figure 13-5. Load-displacement curves showing the evolution of the hysteretic elastic behavior with increasing damage

nature of human bone. The stiffness $K_{i,j}$ is extracted from the slope of load-displacement curves. Only very near failure can one easily measure hysteresis.

Figure 13-3 shows sample resonance curves at increasing drive level $R_{i,j}$, at damage step 0 ($R_{0,j}$) before damage cycling commenced, and at damage step, 8 ($R_{8,j}$), well into the damage process. Clearly, Δf is more pronounced at step $i = 8$, meaning the associated $\alpha_{8,j} > \alpha_{0,j}$. This is quantified in Fig. 13-6, which shows the (frequency normalized) dependence of the resonance curve peaks as a function of drive amplitude, from the data shown in Fig. 13-3. What is clear is that at damage step 0, there is little change in the resonance peak frequency with amplitude; however, at step 8, a measurable change can be seen. From such curves, $\alpha_{i,j}$ can be extracted for each damage step (i) and sample (j).

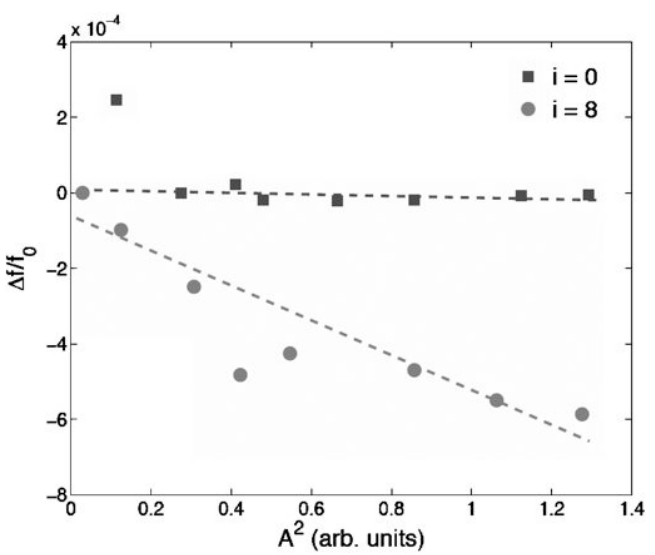

Figure 13-6. Normalized shift of the resonance frequency for the resonance peaks, shown in Fig. 13-3, as a function of the square of the resonance peak amplitude ($A^2 \propto \varepsilon^2$). Dashed lines are shown to more clearly illustrate the trends

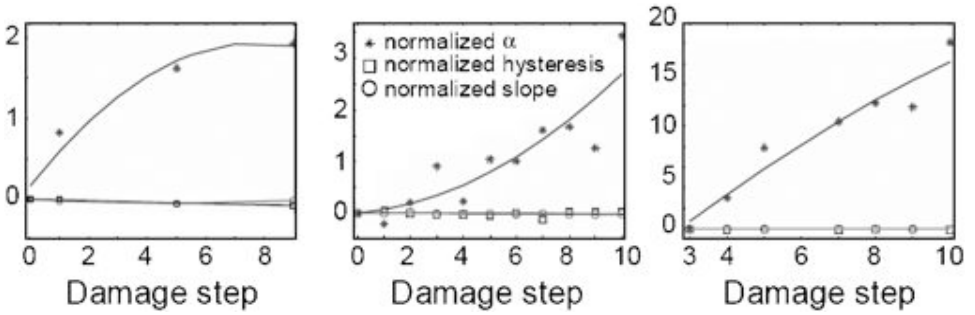

Figure 13-7. Comparison of the non-linear parameter α to the quasi-static load-displacement measures of hysteresis loop area and change in elastic stiffness (i.e., the slope of load-displacement curves) for three samples. All values are normalized to the corresponding value at damage step 0. Note the dramatic increase in the non-linear parameter while the other quantities remain almost unchanged

In Fig. 13-7, normalized α ($\alpha_{i,j}/\alpha_{0,j}$) as a function of damage step i is shown for three samples. The normalized slope of the load-displacement curve, proportional to the stiffness ($K_{i,j}/K_{0,j}$) and the normalized hysteresis ($H_{i,j}/H_{0,j}$) are shown for comparison. The striking result is the fact that there is immeasurable change in the normalized slope and hysteresis, but $\alpha_{i,j}/\alpha_{0,j}$ "sees" the effect of damage cycling very early on, and grows markedly with each damage session. Note that error bars are not shown, but based on repeatability measurements, conducted before the sequence began, and they are on the order of the symbol size. Figure 13-8 shows $\alpha_{i,j}/\alpha_{0,j}$ as a function of damage step for all data collected, in a semi-log plot. Note that there is significant variation in the response, and this is attributed to some or all of the variation to age differences in the sample population (see below). A significant observation is that all samples show $\alpha_{i,j}/\alpha_{0,j}$ increasing as a function

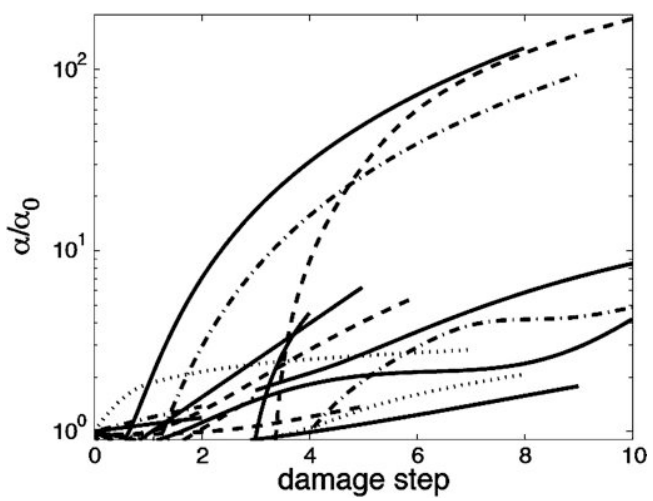

Figure 13-8. Normalized α values for all samples. Trend lines are shown as taken from the original data using smoothing splines. Note the enormity of the variations in the given population

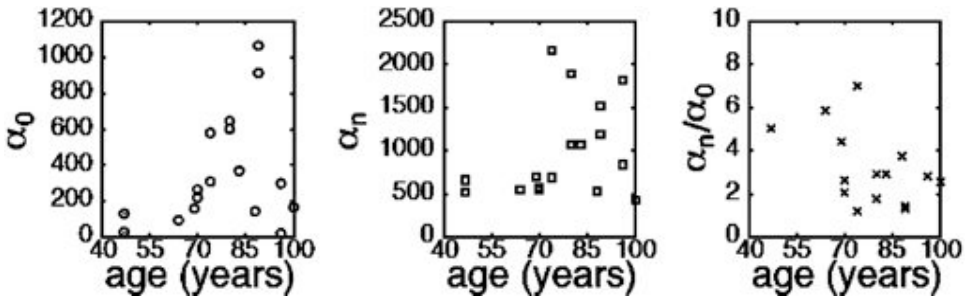

Figure 13-9. Influence of age on the non-linear parameter α (a) before induced fatigue damage, and (b) just before fracture. (c) Ratio of final α_n to initial α_0 values, providing an estimation of the quantity of damage induced before fracture. The few cases where the increase in α was considerably higher (i.e., $\alpha_n/\ \alpha_0 \geq 100$, see Fig. 13-8) are not visible due to the scale

of damage step, and that the stiffness $K_{i,j}/K_{0,j}$ and hysteresis $H_{i,j}/H_{0,j}$ show very little, if any, change with increased damage.

Figure 13-9 shows absolute values of $\alpha_{0,j}$ and $\alpha_{n,j}$ as a function of the sample age, here $n = 7, \ldots, 10$ depending on the sample j and indicates the final damage step completed before failure of the sample occurred. In the event that the sample did not reach catastrophic failure, the value of n was taken as the final damage state, i.e., $n = 10$. The spread in the data is large, and the authors infer that this reflects initial damage state in the population. The spread apparently increases with age; however, since the number of young donors is small, this observation should be treated with caution. Also shown in this figure are the ratios $\alpha_{n,j}/\alpha_{0,j}$ as a function of donor age. This plot shows how much α changed over the duration of the experiment. On average, $\alpha_{n,j}/\ \alpha_{0,j}$ increased by about 2.5 times, but in some cases, far more (see caption).

13.5.2 NWMS Observations

In Fig. 13-10, the observations of loading for all damage sessions in the sample used for the NWMS study are shown [56]. It can be observed that an evolution of the sample length is present (i.e., a permanent compressional deformation); however, due to imperfections of the sample reinsertion into the load frame, as well as the possible presence of the bonding material (a residual from bonding to the transducer) remaining on the samples, this change in sample length was not used in any way for analysis. The load-displacement data was used solely for the extraction of linear fits to extract the stiffness K_i (in an identical fashion as was done for the NRUS study) after each damage session from which normalized parameters are calculated and displayed. The imprecision of the quasi-static displacement measurements X_i prevented the observation of any quasi-static hysteresis.

In Fig. 13-11, an expanded view of the frequency spectrum about the continuous wave frequency is shown. Spectra from two steps are shown, $i = 0$ and 5. The notable difference between the two spectra is the emergence of sideband energy (solid line) around the continuous wave frequency. In contrast, at $i = 0$ there is no measurable sideband energy. This observation is indicative of the enhanced non-linear response with damage cycling. The non-linear parameter Γ_i is obtained from the integral in the frequency range shown in Fig. 13-11, excluding the continuous wave frequency peak (~221 kHz to 225 kHz).

Figure 13-12 shows comparison of the normalized Γ (Γ_i/Γ_0) with normalized K (K_i/K_0) obtained from all damage sessions. Clearly, the non-linear response is far more sensitive

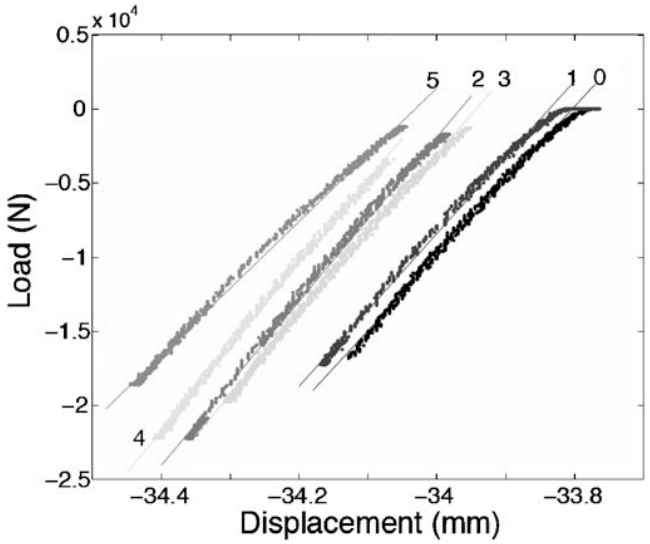

Figure 13-10. Load vs. displacement for each damage step. A linear fit has been applied to extract relative changes in the stiffness *K* (proportional to Young's modulus) as the fatigue damage progressed

to mechanical property change than the stiffness measure, as was also seen in the NRUS experiments (see Fig. 13-7). The respective changes are about 700% and 10%, respectively. Error bars are not noted, but are much smaller than the overall changes. The normalized α and β parameters follow a similar trend to Γ (see Fig. 13-13), as would be expected since Γ

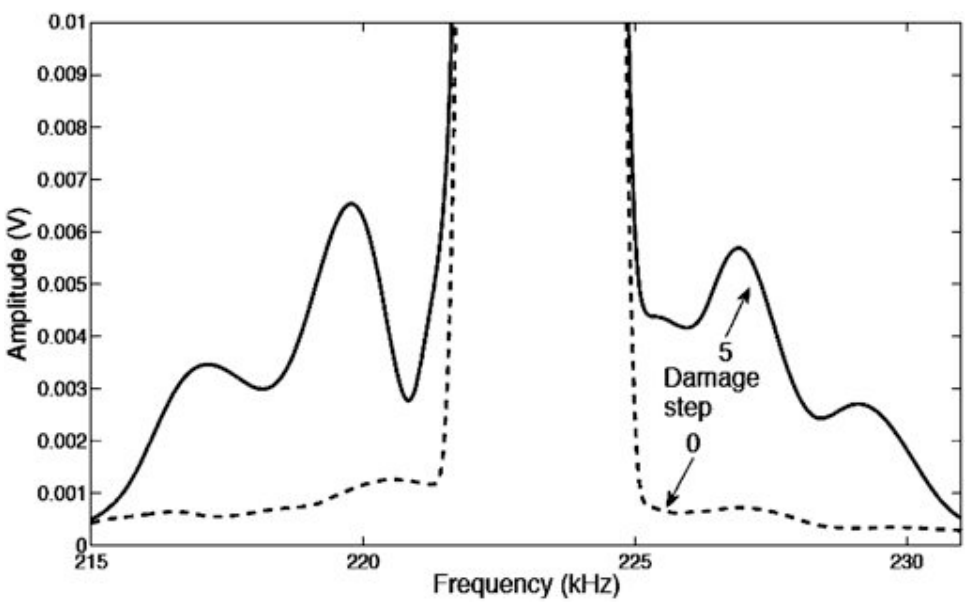

Figure 13-11. Power spectra of sideband frequency range for two damage steps (0 and 5). The increase in sideband energy after fatigue damage has been introduced is clearly visible. The calculation of Γ is done in the frequency range shown (i.e., 215–231 kHz). For the calculation, the central peak at 223 kHz (i.e., ~221–225 kHz) is removed

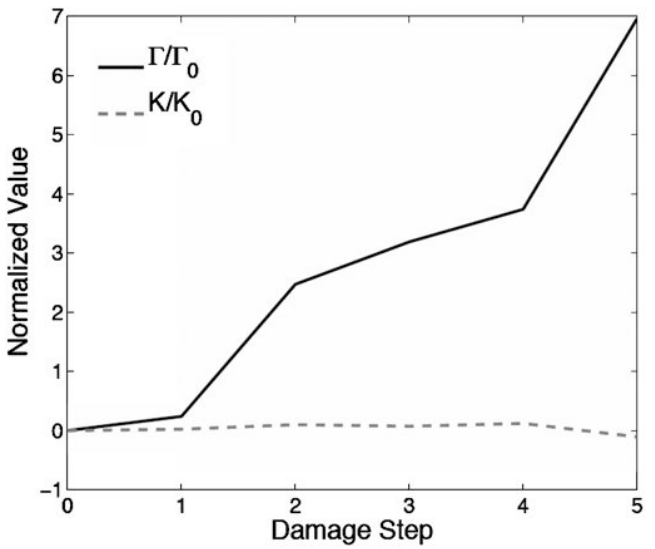

Figure 13-12. Comparison of the relative changes of the non-linear parameter Γ with the relative change in modulus (extracted from linear elastic measurements). Note the almost 700% change in the non-linear parameter Γ, compared to the 10% change in K

must be a function of both α and β. Alone, α and β are more sensitive to damage by roughly an order of magnitude; however, they are more difficult to measure precisely and therefore the errors can be much larger.

Figure 13-14 illustrates how the values in Fig. 13-13 are obtained. Equations (13-1) and (13-2) state that the first- and second-order sidebands, associated with β_i and α_i, respectively, are linearly proportional to the product of the fundamental frequency amplitudes, e.g., $A_{f1\pm f2} \propto \beta A_{f1} A_{f2}$ and $A_{f1\pm 2f2} \propto \alpha A_{f1} A_{f2}$. Here, A is used instead of absolute ε, as absolute

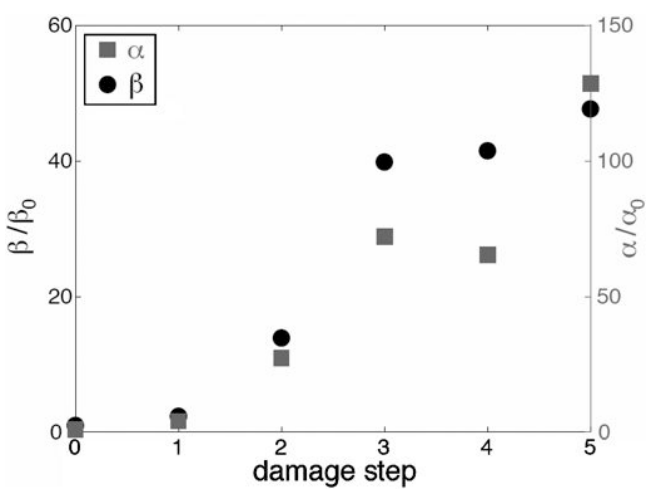

Figure 13-13. Relative changes in the non-linear parameters α (squares) and β (circles). Both non-linear parameters are more sensitive than the parameter Γ introduced above; however, the ease of extracting either α or β from experimental data is for more difficult to do with adequate precision and certainty compared to the calculation of Γ

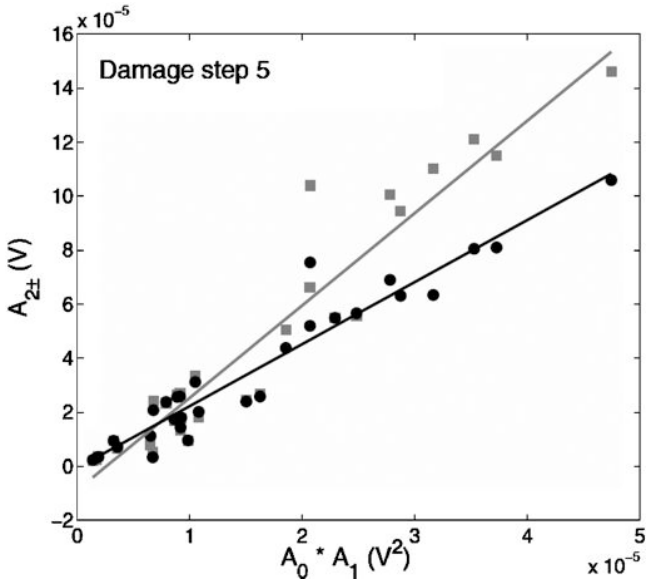

Figure 13-14. Example of second-order sideband amplitudes (e.g., f_{--} = 217 and f_{++} = 230 kHz in Fig. 13-11) as a function of the product of the source amplitudes after the final damage step. The non-linear parameters β and α are extracted from linear fits of such data sets of the first-order and second-order sidebands, respectively

values were not measured. Using all 30 excitation combinations available in each W_i, it is possible to extract the non-linear parameters from a linear fit of the appropriate sideband amplitude versus the product of the excitation amplitudes. As there is no mathematical distinction between amplitudes of sum and difference frequencies (e.g., $f_+ = f_1 + f_2$ and $f_- = f_1 - f_2$, respectively), it should be possible to extract two identical values for α and β from, i.e., one from the sum frequency f_+ and one from the difference frequency f_-. In reality it is not uncommon to obtain two different values (e.g., β_+ and β_-), depending on the use of f_+ or f_-, although the reason for this difference is not understood. This is one of the difficulties in determining one absolute α or β value. To obtain one value here, both values (e.g., α_+ and α_-, as shown in Fig. 13-14) were calculated and the average of the two was taken as the "single" value.

13.6 DISCUSSION AND CONCLUSIONS

In this work, an overview of two non-linear dynamical methods that are derived from non-linear elastic wave spectroscopy is presented, as applied to human bone samples in vitro, in order to demonstrate their viability as a damage diagnostic. The first method, known as non-linear resonant ultrasound spectroscopy, was applied to 18 donor samples that were progressively fatigued. Before the fatigue cycling commenced the non-linear parameter α was obtained. For comparison, quasi-static stiffness and, where possible, hysteresis were measured from the load-displacement curves, quantities that are commonly applied for the measurement of the mechanical state of the material. These measurements provided a baseline in order to characterize the initial state of the samples. The samples were then subject to ten damage sessions in a mechanical load frame, in order to progressively induce mechanical damage. Between each damage session, the same measurements of α, quasi-static stiffness and hysteresis were made. A number of samples failed before the ten sessions were applied. However, despite this, the data trends are clear.

In Figs. 13-7 and 13-8, it has been shown that the non-linear parameter α is extremely sensitive to progressive damage, in contrast to quasi-static stiffness and hysteresis. Figure 13-7 shows that α responds dramatically to the increased damage state within the first two cycling sessions, and by the last session, may increase many hundreds of times. In contrast, the quasi-static stiffness and hysteresis remain essentially unchanged, insensitive to the increasing damage intensity. Figure 13-8 shows results of α from the entire suite of samples. From this plot, it is clear that, (a) α increases as a function of induced damage intensity for all samples, and (b) that there exists a large range in individual responses. The results suggest that the non-linear response *must* be related to the damage intensity. In Fig. 13-9, α has been shown as a function of donor age. The authors infer that these data illustrate that the population distribution of damage intensity before damage cycling commenced, suggesting that there is a large variation in the "damage state" of human bone that may depend on age and other factors. The observations of α as function of age and as a function of progressively induced damage underscore the differences in bone integrity in the population. Confidence in relating non-linear response to progressive damage, and in fact, correlating non-linear response with damage in general, is based on numerous studies relating these quantities in non-biologic materials. Studies that show the same trends as those measured here, include work by Morris et al [58], where progressive damage was induced by bending in high-strength aluminum; Nagy [57], who observed progressive damage from bending in samples of aluminum alloy, polymers, titanium matrix composite, and adhesive layers; Van Den Abeele and De Visscher [59], who observed progressive damage induced by three-point bending in concrete; as well as work that the authors have conducted in, for instance, progressive damage in tension-cycled samples of steel (unpublished). These and many other studies support this interpretation.

This chapter has also described a second NEWS method, known as non-linear wave modulation spectroscopy. This method relies on the non-linear-induced wave multiplication of two or more elastic waves at different frequencies. When the vibration spectrum, induced by an impulsive forcing, is mixed with a pure frequency, continuous wave, the method is perhaps the most robust NEWS method in existence. A hybrid of this method has been shown, where the sidebands in the frequency domain are integrated in order to obtain Γ a function of α and β from Eqs. (13-1) and (13-2). This result is shown in Fig. 13-12, where the result is compared with the stiffness obtained quasi-statically. Like the NRUS results comparing α to stiffness for three samples shown in Fig. 13-7, the non-linear response shows the sensitivity to damage early on (after the first damage session), changing by nearly 700% in contrast to the 10% change in the stiffness.

The observations suggest that if the method is to be successfully applied in vivo, statistics relating Γ, α, and/or β to bone damage will be very important. In future studies, it is clear that empirical relations between measured crack characteristics (e.g., crack density, length, orientation) and non-linear response will have to be developed in order to quantitatively assess damage for both in vitro and in vivo studies. The results also suggest that the method may be of value in following one individual as a function of time if in vivo application is realized.

The samples used in the work presented here had fluids removed from the samples before measuring. It is known from previous work that fluids have a large influence on elastic non-linear response (e.g., [64]), so different magnitudes of non-linear parameters than those shown here may be expected in fluid saturated material. Furthermore, inducing sufficient strain amplitudes in order to induce non-linear response in bone in vivo will be challenging. Separating bone non-linearity from tissue non-linearity should not be a serious issue because tissue non-linearity is significantly smaller than that observed in bone, and exhibits no hysteretic term (α). That is, unless the bone non-linear response is much diminished in vivo. Moreover, measuring the signals in vivo presents its own difficulties due to wave dissipation through tissue. The authors are currently are designing methods to overcome these problems, and intend to begin in vivo studies in the near future.

References

[1] Cornelissen, P., Cornelissen, M., Van der Perre, G., Christensen, A. B., Ammitzboll, F., and Dyrbye, C., 1986, "Assessment of Tibial Stiffness by Vibration Testing in situ — II. Influence of Soft Tissues, Joints and Fibula," *Journal of Biomechanics*, **19**, pp. 551–561.

[2] Jurist, J. M., 1970, "In Vivo Determination of the Elastic Response of Bone. I. Method of Ulnar Resonance Frequency Determination," *Physics in Medicine and Biology*, **15**, pp. 417–426.

[3] Jurist, J. M., 1970, "In Vivo Determination of the Elastic Response of Bone. II. Ulnar Resonant Frequency in Osteoporotic, Diabetic and Normal Subjects," *Physics in Medicine and Biology,* **15**, pp. 427–434.

[4] Van der Perre, G., Van Audekercke, R., Martens, M., and Mulier, J. C., 1983, "Identification of in Vivo Vibration Modes of Human Tibiae by Modal Analysis," *Journal of Biomechanical Engineering*, **105**, pp. 244–248.

[5] Cornelissen, P., Cornelissen, M., Van der Perre, G., Christensen, A. B., Ammitzboll, F., and Dyrbye, C., 1987, "Assessment of Tibial Stiffness by Vibration Testing in Situ — III. Sensitivity of Different Modes and Interpretation of Vibration Measurements," *Journal of Biomechanics*, **20**, pp. 333–342.

[6] Thomas, A. M., Luo, D. Z., and Dunn, J. W., 1991, "Response of Human Femur to Mechanical Vibration," *Journal of Biomedical Engineering*, **13**, pp. 58–60.

[7] Lowet, G., Van Audekercke, R., Van der Perre, G., Geusens, P., Dequeker, J., and Lammens, J., 1993, "The Relation Between Resonant Frequencies and Torsional Stiffness of Long Bones in Vitro. Validation of a Simple Beam Model," *Journal of Biomechanics*, **26**, pp. 689–696.

[8] Couteau, B., Hobatho, M. C., Darmana, R., Brignola, J. C., and Arlaud, J. Y., 1998, "Finite Element Modelling of the Vibrational Behaviour of the Human Femur Using CT-Based Individualized Geometrical and Material Properties," *Journal of Biomechanics*, **31**, pp. 383–386.

[9] Van der Perre, G., and Lowet, G., 1994, "Vibration, Sonic and Ultrasonic Wave Propagation Analysis for the Detection of Osteoporosis," *Clinical Rheumatology*, **13** (Suppl. 1), pp. 45–53.

[10] Van Der Perre, G., and Lowet, G., 1996, "In Vivo Assessment of Bone Mechanical Properties by Vibration and Ultrasonic Wave Propagation Analysis," *Bone*, **18** (Suppl. 1), pp. 29S–35S.

[11] Panteliou, S. D., Abbasi-Jahromi, H., Dimarogonas, A. D., Kohrt, W., and Civitelli, R., 1999, "Low-Frequency Acoustic Sweep Monitoring of Bone Integrity and Osteoporosis," *Journal of Biomechanical Engineering*, **121**, pp. 423–431.

[12] Christopoulou, G. E., Stavropoulou, A., Anastassopoulos, G., Panteliou, S. D., Papadaki, E., Karamanos, N. K., and Panagiotopoulos, E., 2006, "Evaluation of Modal Damping Factor as a Diagnostic Tool for Osteoporosis and Its Relation with Serum Osteocalcin and Collagen I N-Telopeptide for Monitoring the Efficacy of Alendronate in Ovariectomized Rats," *Journal of Pharmaceutical and Biomedical Analysis*, **41**, pp. 891–897.

[13] Singh, V. R., Yadav, S., and Adya, V. P., 1989, "Role of Natural Frequency of Bone as a Guide for Detection of Bone Fracture Healing," *Journal of Biomedical Engineering,* **11**, pp. 457–461.

[14] Tower, S. S., Beals, R. K., and Duwelius, P. J., 1993, "Resonant Frequency Analysis of the Tibia as a Measure of Fracture Healing," *Journal of Orthopaedic Trauma*, **7**, pp. 552–557.

[15] Benirschke, S. K., Mirels, H., Jones, D., and Tencer, A. F., 1993, "The Use of Resonant Frequency Measurements for the Noninvasive Assessment of Mechanical Stiffness of the Healing Tibia," *Journal of Orthopaedic Trauma*, **7**, pp. 64–71.

[16] Nakatsuchi, Y., Tsuchikane, A., and Nomura, A., 1996, "The Vibrational Mode of the Tibia and Assessment of Bone Union in Experimental Fracture Healing Using the Impulse Response Method," *Medical Engineering & Physics*, **18**, pp. 575–583.

[17] Lowet, G., Dayuan, X., and Van der Perre, G., 1996, "Study of the Vibrational Behaviour of a Healing Tibia Using Finite Element Modelling," *Journal of Biomechanics*, **29**, pp. 1003–1010.

[18] Christensen, A. B., Ammitzboll, F., Dyrbye, C., Cornelissen, M., Cornelissen, P., and Van der Perre, G., 1986, "Assessment of Tibial Stiffness by Vibration Testing in Situ — I. Identification of Mode Shapes in Different Supporting Conditions," *Journal of Biomechanics*, **19**, pp. 53–60.

[19] Alizad, A., Walch, M., Greenleaf, J. F., and Fatemi, M., 2006, "Vibrational Characteristics of Bone Fracture and Fracture Repair: Application to Excised Rat Femur," *Journal of Biomechanical Engineering*, **128**, pp. 300–308.

[20] Nikiforidis, G., Bezerianos, A., Dimarogonas, A., and Sutherland, C., 1990, "Monitoring of Fracture Healing by Lateral and Axial Vibration Analysis," *Journal of Biomechanics*, **23**, pp. 323–330.

[21] Roberts, S. G., and Steele, C. R., 2000, "Efficacy of Monitoring Long-Bone Fracture Healing by Measurement of Either Bone Stiffness or Resonant Frequency: Numerical Simulation," *Journal of Orthopaedic Research*, **18**, pp. 691–697.

[22] Rosenstein, A. D., McCoy, G. F., Bulstrode, C. J., McLardy-Smith, P. D., Cunningham, J. L., and Turner-Smith, A. R., 1989, "The Differentiation of Loose and Secure Femoral Implants in Total Hip Replacement Using a Vibrational Technique: An Anatomical and Pilot Clinical Study," *Proceedings of the Institution of Mechacnical Engineers [H]*, **203** (2), pp. 77–81.

[23] Rowlands, A., Duck, F. A., and Cunningham, J. L., 2007 (Jun 21), "Bone Vibration Measurement Using Ultrasound: Application to Detection of Hip Prosthesis Loosening," *Medical Engineering & Physics*, [Epub ahead of print].

[24] Denayer, I., Jaecques, S. V., Burny, F., Puers, R., Borgwardt, A., and Van der Perre, G., 2000, "Measurement of Implant Stability and Osseointegration: Non-Linearities and Resonance Frequencies," *12th Conference European Society of Biomechanics*, Dublin, p. 151.

[25] Cawley, P., Pavlakovic, B., Alleyne, D. N., George, R., Back, T., and Meredith, N., 1998, "The Design of a Vibration Transducer to Monitor the Integrity of Dental Implants," *Proceedings of the Institution of Mechacnical Engineers [H]*, **212**, pp. 265–272.

[26] Njeh, C. F., Hans, D., Fuerst, T., Glüer, C. C., and Genant, H. K. 1999, *Quantitative Ultrasound: Assessment of Osteoporosis and Bone Status*, Martin Dunitz, London, United Kingdom, 1999.

[27] Siegel, I. M., Anast, G. T., and Fields, T., 1958, "The Determination of Fracture Healing by Measurement of Sound Velocity Across the Fracture Site," *Surgery, Gynecology & Obstetrics*, **107**, pp. 327–332.

[28] Langton, C. M., Palmer, S. B., and Porter, R. W., 1984, "The Measurement of Broadband Ultrasonic Attenuation in Cancellous Bone," *Engineering in Medicine*, **13**, pp. 89–91.

[29] Marin, F., Gonzalez-Macias, J., Diez-Perez, A., Palma, S., and Delgado-Rodriguez, M., 2006, "Relationship Between Bone Quantitative Ultrasound and Fractures: A Meta-Analysis," *Journal of Bone and Mineral Research*, **21**, pp. 1126–1135.

[30] Laugier, P., Droin, P., Laval-Jeantet, A. M., and Berger, G., 1997, "In Vitro Assessment of the Relationship Between Acoustic Properties and Bone Mass Density of the Calcaneus by Comparison of Ultrasound Parametric Imaging and Quantitative Computed Tomography," *Bone*, **20**, pp. 157–165.

[31] Nicholson, P. H., Muller, R., Cheng, X. G., Ruegsegger, P., Van Der Perre, G., Dequeker, J., and Boonen, S., 2001, "Quantitative Ultrasound and Trabecular Architecture in the Human Calcaneus," *Journal of Bone and Mineral Research*, **16**, pp. 1886–1892.

[32] Raum, K., Leguerney, I., Chandelier, F., Bossy, E., Talmant, M., Saied, A., Peyrin, F., and Laugier, P., 2005, "Bone Microstructure and Elastic Tissue Properties Are Reflected in QUS Axial Transmission Measurements," *Ultrasound in Medicine and Biology*, **31**, pp. 1225–1235.

[33] Nicholson, P. H., Bouxsein, M. L., 2000, "Quantitative Ultrasound Does Not Reflect Mechanically Induced Damage in Human Cancellous Bone," *Journal of Bone and Mineral Research*, **15**, pp. 2467–2472.

[34] Martin, B., 1993, "Aging and Strength of Bone as a Structural Material," *Calcified Tissue International*, **56** (Suppl 1) S34–S39; discussion S39–S40.

[35] Turner, C. H., 2002, "Biomechanics of Bone: Determinants of Skeletal Fragility and bone quality," *Osteoporosis International*, **13**, pp. 97–104.

[36] Parfitt, A. M., 1993, "Bone Age, Mineral Density, and Fatigue Damage," *Calcified Tissue International*, **53** (Suppl. 1) S82–S85; discussion S85–S86.

[37] Norman, A. L., and Wang, Z., 1997, "Microdamage of Human Cortical Bone: Incidence and morphology in Long Bones," *Bone*, **20**, pp. 375–379.

[38] Schaffler, M. B., Chio, K., and Milgrom, C., 1995, "Aging and Matrix Microdamage Accumulation in Human Compact Bone," *Bone*, **17**, pp. 521–525.

[39] Martin, R., 2003, "Fatigue Microdamage as an Essential Element of Bone Mechanics and Biology," *Calcified Tissue International*, **73**, pp. 101–107.

[40] Burr, D. B., Forwood, M. R., Fyhrie, D. P., Martin, R. B., Schaffler, M. B., and Turner, H. C., 1997, "Bone Microdamage and Skeletal Fragility in Osteoporotic and Stress Fractures," *Journal of Bone and Mineral Research*, **12** (1), pp. 9–15.

[41] Zioupos, P., 2001, "Accumulation of *in Vivo* Fatigue Microdamage and Its Relation to Biomechanical Properties in Aged Human Cortical Bone," *Journal of Microscopy*, **201** (Pt2), pp. 270–278.

[42] Schaffler, M. B., Radin, E. L., and Burr, D. B., 1989, "Mechanical and Morphological Effects of Strain Rate on Fatigue of Compact Bone," *Bone*, **10**, pp. 207–214.

[43] Fazzalarin, N. L., Forwood, M. R., Smith, K., Manthey, B. A., and Herreen, P., 1998, "Assessment of Cancellous Bone Quality in Severe Osteoarthrosis: Bone Mineral Density, Mechanics, and Microdamage," *Bone*, **22**, pp. 381–388.

[44] Burr, D. B., and Stafford, T., 1990, "Validity of the Bulk Staining Technique to Separate Artifactual from *in Vivo* Bone Microdamage," *Clinical Orthopaedics*, **260**, pp. 305–308.

[45] Lee, T. C., Myers, E. R., and Hayes, W. C., 1998, "Fluorescence Aided Detection of Microdamage in Compact Bone," *Journal of Anatomy*, **193**(Pt 2), pp. 179–184.

[46] Lee, T. C., Arthur, T. L., Gibson, L. J., and Hayes, W. C., 2000, "Sequential Labeling of Microdamage in Bone Using Chelating Agents," *Journal of Orthopaedic Research*, **18**, pp. 322–325.

[47] Thurner, P. J., Wyss, P., Voide, R., Stauber, M., Stampanoni, M., Sennhauser, U., and Muller, R., 2006, "Time-Lapsed Investigation of Three-Dimensional Failure and Damage Accumulation in Trabecular Bone Using Synchrotron Light," *Bone,* **39**, pp. 288–299.

[48] Johnson, P. A., Van Den Abeele, K., TenCate, J., and Guyer, R., Resonant Nonlinear Ultrasound Spectroscopy, US Patent Number 6,330,827, Dec 18, 2001.

[49] Johnson, P. A., "The New Wave in Acoustic Testing," 1999, *Materials World, the J. Inst. Materials*, **7**, pp. 544–546.

[50] Van Den Abeele, K. E.- A., Johnson, P. A., and Sutin, A., 2000, "Nonlinear Elastic Wave Spectroscopy (NEWS) Techniques to Discern Material Damage. Part I: Nonlinear Wave Modulation Spectroscopy (NWMS)," *Research on Nondestructive Evaluation*, **12**, pp. 17–30.

[51] Van den Abeele, K. E.- A., Carmeliet, J., Ten Cate, J. A., and Johnson, P. A., 2000, "Nonlinear Elastic Wave Spectroscopy (NEWS) Techniques to Discern Material Damage, Part II: Single-Mode Nonlinear Resonance Acoustic Spectroscopy," *Research in Nondestructive Evaluation*, **12**, pp. 31–42.

[52] Ostrovsky, L., and Johnson, P. A., 2001, "Dynamic Nonlinear Elasticity in Geomaterials," *Rivista del Nuovo Cimento*, **24**, pp. 1–46.

[53] Johnson, P. A., and Sutin, A., 2005, "Slow Dynamics and Anomalous Nonlinear Fast Dynamics in Diverse Solids," *Journal of the Acoustical Society of America*, 117, pp. 124–130.

[54] Lee, T., Lakes, R. S., and Lal, A., 2002, "Investigation of Bovine Bone by Resonant Ultrasound Spectroscopy and Transmission Ultrasound," *Biomechacnics and Modelling in Mechanobiology*, **1**, pp. 165–175.

[55] Muller, M., Mitton, D., Talmant, M., Laugier, P., and Johnson, P. A., 2007, "Nonlinear Ultrasound Can Detect Accumulated Damage in Human Bone," *J. Biomechanics*, in review.

[56] Ulrich, T. J., Johnson, P., Muller, M., Mitton, D., Talmant, M., and Laugier, P., 2007, "Application of Nonlinear Dynamics to Progressive Fatigue Damage in Human Cortical Bone," *Applied Physics Letters*, in press.

[57] Nagy, P., 1998, "Fatigue Damage Assessment by Nonlinear Ultrasonic Materials Characterization," *Ultrasonics*, **36**, pp. 375–381.

[58] Morris, W. L., Buck, O., and Inman, R. V., 1979, "Acoustic Harmonic Generation Due to Fatigue Damage in High Strength Aluminum," *Journal of Applied Physics*, **50**, pp. 6737–6741.

[59] Van Den Abeele, K., and De Visscher, J., 2000, "Damage Assessment in Reinforced Concrete Using Spectral and Temporal Nonlinear Vibration Techniques," *Cement and Concrete Research*, **30**, pp.1453–1464.

[60] Guyer, R. A., and Johnson, P. A., 1999, "Nonlinear Mesoscopic Elasticity: Evidence for a New Class of Materials," *Physics Today*, **52**, pp. 30–35.

[61] McCall, K. R., and Guyer, R. A., 1994, "Equation of State and Wave Propagation in Hysteretic Nonlinear Elastic Materials," *Journal of Geophysical Research,* **99**, pp. 23887–23897.

[62] Guyer, R. A., McCall, K. R., and Boitnott, G. N., 1995, "Hysteresis, Discrete Memory and Nonlinear Wave Propagation in Rock: A New Paradigm," *Physical Review Letters,* **74**, pp. 3491–3494.

[63] McCall, K. R., and Guyer, R. A., 1996, "Hysteresis, Discrete Memory and Nonlinear Elastic Wave Propagation in Rock: A New Theoretical Paradigm," *Nonlinear Processes in Geophysics*, **3**, pp. 89–101.

[64] Van Den Abeele, K. E.- A., Carmeliet, J., Johnson, P. A., and Zinzsner, B., 2002, "The Influence of Water Saturation on the Nonlinear Mesoscopic Response of Earth Materials, and the Implications to the Mechanism of Nonlinearity," *Journal of Geophysical Research*, **107**, pp. 10,1029–10,1040.

[65] Landau, L. D., and Lifshitz, E. M., 1980, *Theory of Elasticity*, Pergamon, Oxford, United Kingdom, 1980.

[66] Muller, M., Sutin, A., Guyer, R., Talmant, M., Laugier, P., and Johnson, P. A., 2005, "Nonlinear Resonant Ultrasound Spectroscopy (NRUS) Applied to Damage Assessment in Bone," *Journal of the Acoustical Society of America*, **118**, pp. 3946–3952.